Anal. Methods Environ. Chem. J. 8 (3) (2025) 182-204

AMECJ

Research Article, Issue 3
Analytical Methods in Environmental Chemistry Journal
Journal home page: www.amecj.com/ir

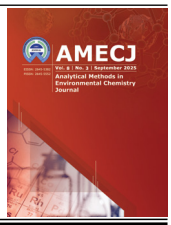

Spectroscopy analysis and computational chemistry: Liquid-assisted mechanochemical synthesis of new heteroleptic copper complexes with pyridine-based Schiff base ligand

Ruchika Jaryal[a,*], Amit Kumar[b], and Shamshad Ahmad Khan[a]
[a]*Chemistry Department, DAV PG College, Siwan841226-, Jai Prakash University, Bihar India*
[b] *Chemistry Department, A N College, Patna800013-, Patliputra University, Bihar India*

ARTICLE INFO:
Received 8 May 2025
Revised form 16 Jul 2025
Accepted 18 Aug 2025
Available online 30 Sep 2025

Keywords:
Spectroscopy analysis,
Chemical ligand,
Heteroleptic complexes,
Liquid-assisted grinding,
Acetylcholinesterase

ABSTRACT
In this study, the Schiff base ligand 4-bromo-2-((pyridine-2-ylimino) methyl) phenol (HL) was prepared by refluxing 2-aminopyridine with 5-bromosalicylaldehyde. The new heteroleptic complexes of HL with copper, [Cu(L)(8HQ)] as complex one and [Cu(L)(phen) Br] as complex two, were synthesized using the liquid-assisted grinding (LAG) method, where 8-Hydroxyquinoline (8HQ) and 1,10-Phenanthroline (phen) served as co-ligands. IR, HRMS, and UV-visible spectroscopy techniques were used to analyze and characterize HL and copper complexes. The copper complexes have a lower HOMO-LUMO energy gap than HL. The Pearson correlation coefficient (r) and P-value indicate that the chosen level of theory is suitable for DFT-based calculations. Molecular docking of acetylcholinesterase (AChE) from Drosophila melanogaster (fruit flies) indicated that HL has the potential to bind at the enzyme's catalytic triad site. The in-silico toxicological study of HL and copper complexes revealed that HL and both complexes are non-AMES toxic and non-carcinogenic. The in vitro analysis results show that HL and complexes are biologically active against Drosophila melanogaster.

1. Introduction

The Schiff base metal complexes are biologically active against fungi, bacteria, and insects [1]. The Schiff bases and their metal complexes showed antinemic activity against the root-knot nematode [2]. Schiff base metal complexes exhibit antioxidant, antibiotic, antifertility properties in insects, antimicrobial properties, and enzyme inhibition capabilities [3,4]. The copper complexes with heterocyclic ligands have insecticidal properties and are highly toxic at the larval phase [5]. The copper complexes have antifungal activity in insects [6]. The microcapsule formulation of copper complex has plant growth regulation properties [7]. The Schiff base metal complexes exhibited enzyme-inhibiting properties against glutathione S-transferase (GST), acetylcholinesterase (AChE), and butyrylcholinesterase (BChE) enzymes [8]. In insects, acetylcholinesterase (AChE) is the target site for several naturally occurring and synthetic insecticides [9]. Most commercially essential insecticides are neurotoxins that inhibit acetylcholinesterase (AChE), including organophosphates, carbamates, spinosad, and neonicotinoid insecticides [10]. The organophosphates and carbamates bind to serine in the active site of the enzyme and inhibit acetylcholinesterases (AChE) [11]. Neonicotinoids

*Corresponding Author: Ruchika Jaryal
Email: ruchika.jaryal@gmail.com
https://doi.org/10.24200/amecj.v8.i03.1033

mimic the action of neurotransmitter acetylcholine (ACh) and work as agonists for acetylcholinesterase (AChE) of the insect brain [12]. Spinosad is primarily an allosteric agonist of insect acetylcholinesterase (AChE) [13]. Pyridine is a critical structural unit of many neonicotinoid insecticides, such as imidacloprid and acetamiprid [14]. The organophosphate insecticide chlorpyrifos contained a substituted pyridine ring in the main framework structure [15]. The insecticides flonicamid and pymetrozine also contain a pyridine ring [16]. The pyridine-based derivatives have insecticidal, herbicidal, plant growth regulator, fungicidal, nematocides, and insect repellent properties [17]. Thus, the pyridine-based compounds have great potential for insecticidal properties. Mechanochemistry is currently recognized as an innovative technology that facilitates the practical and sustainable preparation of organic and inorganic compounds [18]. Mechanochemical methods of synthesis reduce the need for bulk solvents and minimize waste production [19]. The mechanochemical techniques proved successful, whereas solvent-based methods failed due to the poor solubility of the reactants [20]. Liquid-assisted grinding (LAG), also known as the solvent-drop grinding method, is a technique that utilizes a small amount of liquid to enhance or control reactivity. Liquid-assisted grinding (LAG) can produce products with higher crystallinity than those obtained through neat grinding. Mechanochemical methods have been successfully employed for the synthesis of metal-organic frameworks (MOFs) and other metal-organic materials using LAG. Mechanochemical methods have been used to prepare mononuclear and multinuclear coordination complexes [21]. In the present study, a pyridine-based Schiff base ligand (HL) and heteroleptic copper complexes with HL and 8-hydroxyquinoline or 1,10-phenanthroline have been synthesized. The DFT calculations were performed for ligands and complexes to optimize geometries, generate IR spectra, electronic spectra, and electron density maps. To the best of our knowledge, there is no literature available on the molecular docking of pyridine-based Schiff base ligands and their copper complexes with acetylcholinesterase (AChE) from Drosophila melanogaster (fruit flies). We have investigated the insecticidal properties of the ligand (HL) and its copper complexes on acetylcholinesterase (AChE) from Drosophila melanogaster (fruit flies) using the molecular docking method. The docked results are compared with those of the commercially popular acetamiprid insecticide. The in-vitro study for insecticidal bio-efficacy and toxicity was also performed on Drosophila melanogaster.

2. Experimental

2.1. Material and Instrumentation

All the chemicals used in the synthesis were AR-grade. The chemicals 2-aminopyridine (purity > 99%), 5-Bromosalicyaldehyde (purity > 99%), 8-Hydroxyquinoline (purity > 99%), 1,10-Phenanthroline monohydrate (purity > 99%), and copper acetate monohydrate (purity > 95%) were purchased from TCI and used without further purification. Spectroscopic-grade ethanol (purity ≥ 95.0%) and methanol (purity ≥ 99.7%) from CDH Fine Chemical were used during preparation. The EuroVector EA3000 Series was used for elemental detection, with detection limits ranging from 0.1 to 1.0 µg. The sample was weighed in an aluminium container of known weight. The sample was injected into a high-temperature (1000°C) furnace and combusted with pure oxygen, where carbon was converted to carbon dioxide, hydrogen to water, and nitrogen to nitrogen gas/ oxides of nitrogen. A variety of absorbents were used to remove any additional combustion products. The Oxygen content was determined on the same instrument in pyrolysis mode. For the quantification of elements, the high-purity micro-analytical standard nicotinamide was used. Copper residues remained as the ash in an aluminium container. The remaining Bromine content was found by mathematical calculation. A PerkinElmer FT-IR spectrophotometer, with a resolution of 0.5 cm^{-1} to 64 cm^{-1} and five scan accumulations, was used for the IR spectroscopic analysis. The IR spectra

were obtained in the range from 4000 cm^{-1} to 650 cm^{-1}. The absorption spectrum in the UV-visible range was obtained using a Varian Cary-5 UV-visible spectrophotometer. High-resolution mass spectrometry (HRMS) analysis was performed using a Waters Alliance e2695 (Separations Module, an integrated solvent system).

2.2. Synthesis study

2.2.1.Synthesis of Schiff base ligand (HL)

4-bromo-2-((pyridine-2-ylimino) methyl) phenol (HL) was prepared by refluxing 2.0 mmol (0.189 g) of 2-Aminopyridine with 2.0 mmol of 5-Bromosalicyaldehyde (0.408 g) in ethanol (25ml). The refluxing continued for 3 hours, and orange colour precipitates were formed upon cooling. The precipitates were filtered and washed with ethanol: water (3:7). Ethanol was used for recrystallization. The weight of the dried orange powder was recorded. Yield: 0.493 g (89%), colour: Orange, Elemental analysis found (%):C, 51.98; H, 3.25; N, 10.08; O, 5.74; Br, 28.80. $C_{12}H_9N_2OBr$: C, 52.01; H, 3.28; N, 10.11; O: 5.77; Br, 28.83. Selected IR data (KBr, cm^{-1}): 1181.66 (s) ν(C-O),1462.18 (s) ν(C=C),1587.57 (s) ν(C=N), 1610.73 (m) ν(C=N), 3421.73 (s) ν(OH). UV-Vis data in methanol λ_{max} (nm):309 nm ($\pi \rightarrow \pi^*$ due to C=C), 359 nm ($n \rightarrow \pi^*$ due to C=N)

2.2.2.Synthesis of complex one (1)

The (N-(4-bromo-2-((pyridine-2-ylimino)methyl) phenolate)) (8-hydroxyquinolate)-copper (II), as complex one**,** was prepared by the LAG method. 1.0 mmol (0.195 g) of Cu $(OAc)_2.H_20$ was ground manually with 1.0 mmol (0.281 g) of HL and 1.0 mmol (0.147 g) of 8-Hydroxyquinoline in a china dish with a pestle using two drops of methanol. The grinding was continued for 10 minutes, and then the reaction mixture was heated up to 50 °C for a few seconds with continuous grinding. After that, the heat was removed, and grinding was continued for 20 minutes to ensure the reaction was complete. The blue-coloured powder was transferred to filter paper and washed with chloroform to remove the unreacted starting materials. Methanol was used for recrystallization. The weight of the dried powder was recorded**.** Yield: 0.406 g (84%), colour: blue, Elemental analysis found (%): Cu, 13.11; C, 52.10; H, 2.88; N, 8.65; O, 6.66; Br, 16.51, $C_{21}H_{14}N_3O_2CuBr$ calcd.: Cu, 13.13; C, 52.13; H, 2.91; N, 8.68; O, 6.62; Br, 16.53. Selected IR data (KBr, cm^{-1}): 1295.42 (s) ν(C-O), 1469.40 (s) ν(C=C), 1542.09 (s) ν(C=N), 1578.69 (s) ν(C=N). UV-Vis data in methanol λ_{max} (nm):585 (d-d transition).

2.2.3.Synthesis of complex two (2)

The Bromo-(N-(4-bromo-2-((pyridine-2-ylimino) methyl)phenolate)) (1,10-phenanthroline)-copper (II), as complex two, was prepared by the LAG method. In preparation, 1.0 mmol (0.197 g) of Cu $(OAc)_2.H_20$ was ground manually with 1.0 mmol (0.277 g) of HL, 1.0 mmol (0.196 g) of 1,10-Phenanthroline monohydrate, and 1.0 mmol (0.121g) of KBr in a China dish with a pestle using 2.0 drops of methanol. The grinding was continued for 10 minutes and then the reaction mixture was heated up to 50 °C for a few seconds with continuous grinding. After that, the heat was removed, and grinding was continued for 20 minutes to ensure the reaction was complete. The blue-coloured powder was transferred to filter paper and washed with chloroform to remove the unreacted starting materials. Methanol was used for recrystallization. The dried powder weight was recorded**.** Yield: 0.485 g (81%), colour: blue, Elemental analysis found (%): Cu, 10.57; C, 48.04; H, 2.66; N, 9.32; O, 2.65; Br, 26.63, $C_{24}H_{16}N_4OCuBr_2$ calcd.: Cu, 10.59; C, 48.07; H, 2.68; N, 9.35; O, 2.67: Br, 26.64. Selected IR data (KBr, cm^{-1}): 1250.82 (s) ν(C-O), 1468.98(s) ν(C=C),1559.72 (s) ν(C=N),1642.56 ν(C=N). UV-Vis data in methanol λ_{max} (nm): 402 (charge transfer band), 599 (d-d transition)

2.3. Computational Studies

The ORCA version 4.2.1, MOPAC2016, and Multiwfn 3.8 quantum chemistry programs packages were used for DFT-based theoretical calculations [22]. The optimized geometries, FMOs, IR spectra, electronic spectra, and electron density maps of the ligand and copper complexes were computed by

DFT-based calculations. The Becke '88 exchange and Perdew '86 correlation function (BP86) with the basis set def2-SVP was used to obtain FMOs in ORCA software [23]. The FMOs are crucial for predicting the stability of the complexes. The essential parameters related to the FMOs were calculated by using the following relations [24]. The theoretical IR spectra were calculated by the MOPAC2016 software using the RHF method [25]. The Electron Localization (ELF) and Localized Orbital Locator (LOL) plots were computed by the Multiwfn 3.8 wave function analyzer software (Eq.1). The accuracy of the basis set at the given level of function in theoretical calculations for IR spectra was checked by using the pearson correlation coefficient (r) with the *P-value* (Eq.2). The correlation coefficient (r) and the *P-value* are used to compare the experimental results with the theoretical results [26]. The theoretical HRMS of the ligand was obtained using CFM-ID 4.0 software, and the file was input in SMILES format to obtain the result.

$$\chi = \frac{(I + A)}{2};\ \omega = \mu^2/(2\,\eta)$$

(Eq.1)

$$r = \frac{\sum(x_i - \bar{x})(y_i - \bar{y})}{\sqrt{\sum(x_i - \bar{x})^2 \sum(y_i - \bar{y})^2}}$$

(Eq.2)

Ionization energy I = - E_{HOMO}, electron affinity A = -$E_{LUMO,}$ energy gap (ΔE) = E_{LUMO} - E_{HOMO}, chemical softness (σ) = $\frac{1}{\eta}$. Also, chemical potential (μ) = -χ and chemical hardness calculated by (η) = $\frac{\Delta E}{2}$. The electrophilicity index and the electronegativity are (ω) and (χ), respectively, and are calculated in Equation 1. Additionally, the correlation coefficient (r) was calculated using Equation 2. The correlation coefficient (r) is shown below for the relevant parameters.

x_i = values of the x-variables in the experimental result

$\bar{x}$ = mean of the values of the x-variable

y_i = values of the y-variable in the theoretical result

$\bar{y}$ = mean of the values of the y-variables.

2.4. Molecular docking and pharmacokinetic studies

The AutoDock Vina software was used for target-specific molecular docking to simulate the interaction of the ligand and complexes with the protein of acetylcholinesterase from Drosophila melanogaster (PDB: 6XYS) [27]. The Siwss-Pdb Viewer software was used to remove the bonded organic molecules at the active site of the protein [28]. The target-specific docking was performed at the pocket containing catalytic triad residues (Glu367/His480/Ser238) along with residues of the peripheral site (Trp321), acyl-binding pocket (Trp271), and choline-binding pocket (Trp83). Discovery Studio Visualizer software was used to visualize the docking results [29,30]. An in-silico study of physicochemical parameters and toxicity in HL and copper complexes was conducted using the SwissADME software and AdmetSAR software [31].

2.5. In-vitro test for insecticidal bio-efficacy and toxicity

For the determination of LD50 values of HL and metal complexes, 150 adults of Drosophila melanogaster were divided into fifteen groups. Each group consisted of ten male/female flies at the age of 2-3 days. All flies were fed with standard food before the mortality assay testing. Drosophila melanogaster was exposed to various concentrations of HL and metal complexes prepared in methanol along with the diet. After 24 hours of treatment, mortality was recorded, and LD50 values were calculated using the arithmetic Karber method, as described in Equation 3 [32].

$$LD_{50} = LD_{100} - \sum \frac{a \times b}{n}$$

(Eq.3)

LD_{50} = Median lethal dose

LD_{100} = The least dose required to kill 100%

a = dose difference

b = mean mortality

n = group population

3. Result and Discussion

3.1. Synthesis and Characterization

The synthesis of complexes is shown in Scheme 1. The refluxing method is preferred for the formation of heterocyclic Schiff base compared to a general acid-catalysed reaction because acid catalysis can deactivate the heterocyclic ring [33]. In liquid-assisted grinding (LAG), the small amount of liquid facilitates the formation of co-crystals and enhances the reaction rate. The heating of the reaction mixture in the LAG method helped in the formation of pure coordination complexes [34].

3.2. IR spectral studies

The IR spectrum of ligand HL is shown in Schema 2. The wavenumbers 1181.66 cm^{-1}, 1276.09 cm^{-1}, 1345.67 cm^{-1} represent bending vibration modes of aromatic rings in HL, and wavenumbers 1462.18 cm^{-1}, 1587.57 cm^{-1} show the stretching vibration modes of C=C and C=N of aromatic rings in HL, respectively [35]. The imine bond stretching occurred at 1610.73 cm^{-1}, and the O-H bond stretching vibration occurred at 3421.73 cm^{-1} in the spectra [36]. IR spectra of the copper complexes are shown in Schemes 3 and 4. The O-H stretching vibration is absent in the copper complexes' spectra, which confirms the bonding through the phenolic side of the ligand. The imine bond stretching occurred at 1578.69 cm^{-1} in complex one and at 1559.72 cm^{-1}in complex two. There is a decrease in the imine stretching vibration in copper complexes compared to the ligand. This indicates coordination through the N side of the imine bond, which lowers the force constant value for C=N [37]. For the complex one, the aromatic stretching vibration ν(C=N) in 8-Hydroxyquinoline occurred at 1542.09 cm^{-1}, and in complex two, the aromatic stretching vibration ν(C=N) in 1,10-Phenanthroline occurred at 1642.56 cm^{-1}. These values indicate the coordination through the N atom of the heterocyclic co-ligands [38]. In HL, the C-O stretching of the aromatic ring appeared at 1181.66 cm^{-1}. The coordination with the metal ion shifted the C-O stretching frequency towards higher wave numbers. The C-O stretching in complex one is at 1295.42 cm^{-1} and in complex two is at 1250.82 cm^{-1}, which is higher than the ligand and confirms Cu-O bonding in the complexes [39].

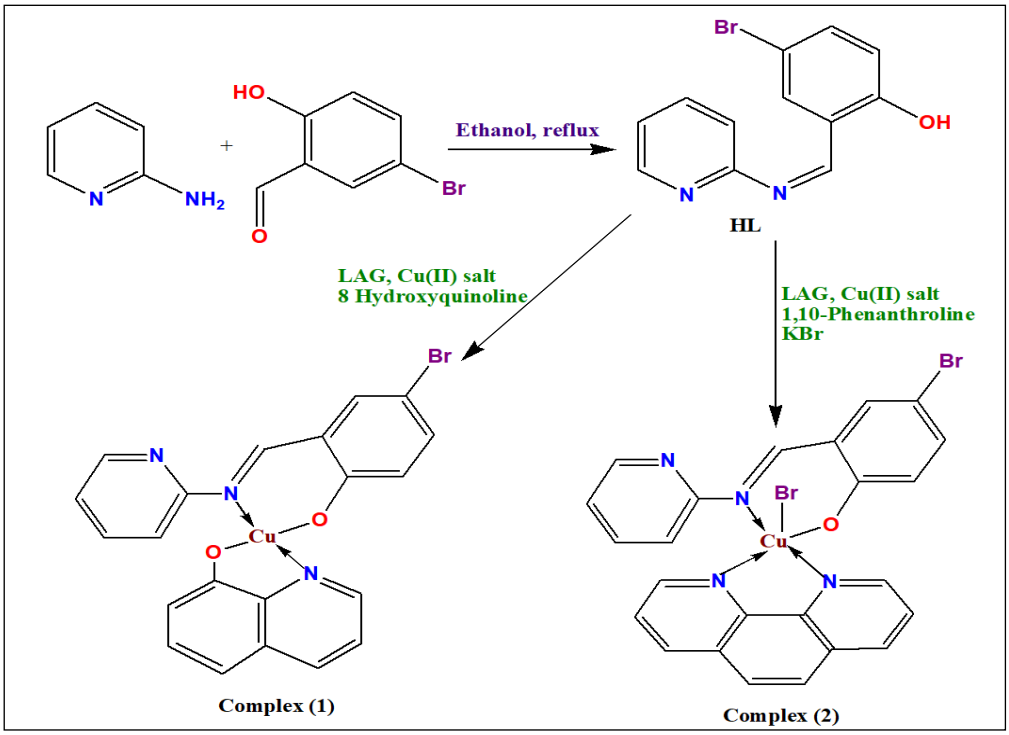

Scheme 1. Synthesis of HL, [Cu(L)(8HQ)] complex one and [Cu(L)(phen)Br] complex two

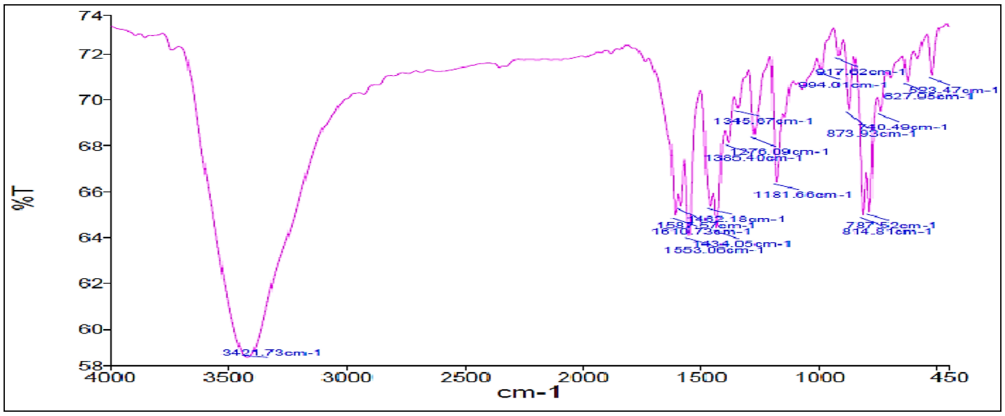

Schema 2. Experimental IR spectrum of ligand HL

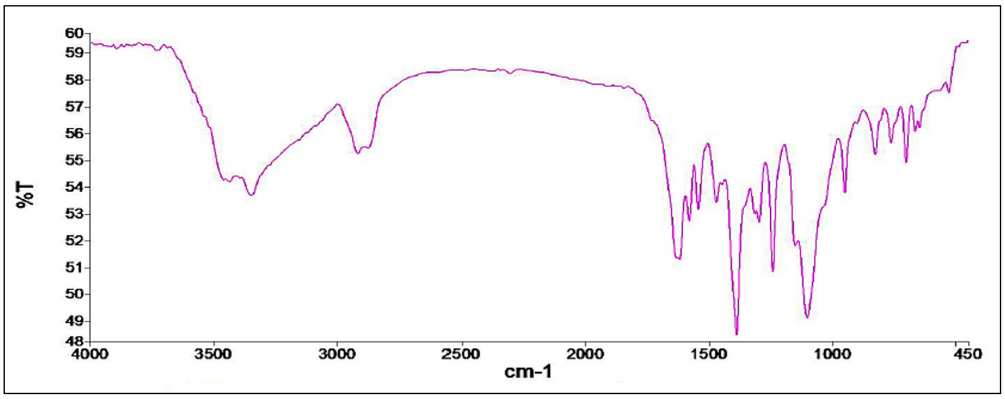

Schema 3. Experimental IR spectra of complex one

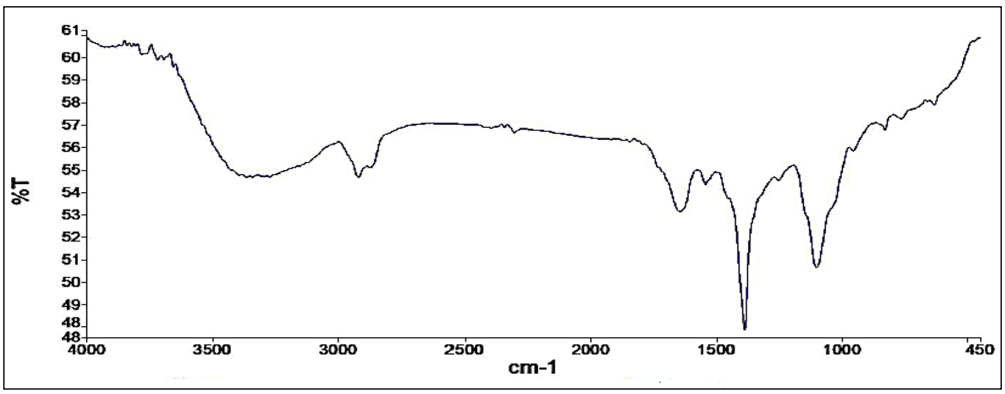

Schema 4. Experimental IR spectra of complex two

3.3. UV-Visible spectral studies

The metal complexes are shown in Figure 1a, and the UV-Visible spectra of the HL are shown in Figure 1b. The spectra of HL exhibit a broad, split peak with two maxima at 309 nm and 359 nm, extending up to 450 nm in the visible region. The peaks are due to π→ π∗ transition in C=C of the phenyl ring and n→ π∗ transition in C=N of the HL. The copper complexes have absorption in the visible region. The absorption maxima for complex one and complex two are 585 nm and 599 nm, respectively. The experimental absorption spectra of the complexes in solution exhibit a single broad and weak absorption band due to the d-d transition [40]. The d-d transitions in metal complexes required less energy for transitions, and absorption bands appeared at higher wavelengths of the visible region. The MLCT absorption bands appeared at a lower wavelength in the visible region. The intensities of MLCT bands are higher than those of d-d transitions [41].

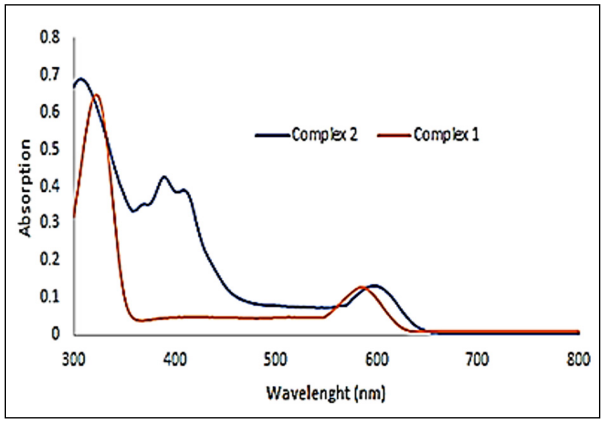

Fig. 1a. Spectra of Cu complexes in methanol

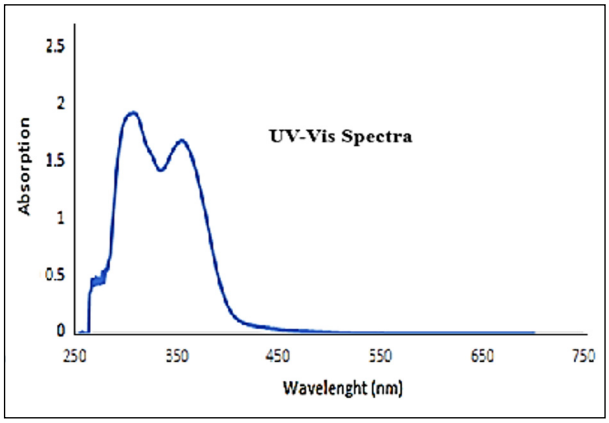

Fig. 1b. UV- visible spectra of HL

3.4. Mass spectral analysis

HRMS data of the ligand HL is shown in Figure 2. The presence of a molecular ion peak at m/z 277.32 confirmed the formation of HL. The molecular peak cluster in the brominated HL reflects the relative abundance of the bromine isotopes. The HRMS data of complex one and complex two are depicted in Figures 3 and 4, respectively. The base peak in complex one is at m/z 479.51, and in complex two is at m/z 181.1, representing the ion with the highest abundance. The presence of molecular ion peaks in the mass data of complexes confirmed the formation of the complexes [42].

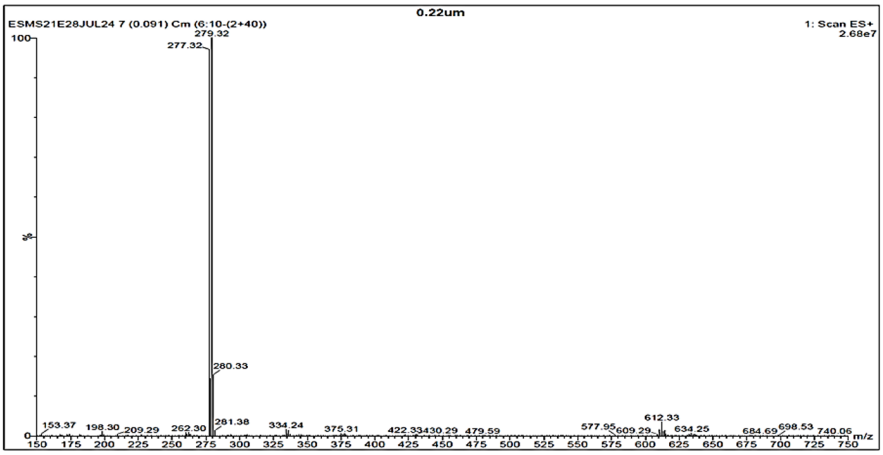

Fig. 2. HRMS of ligand HL

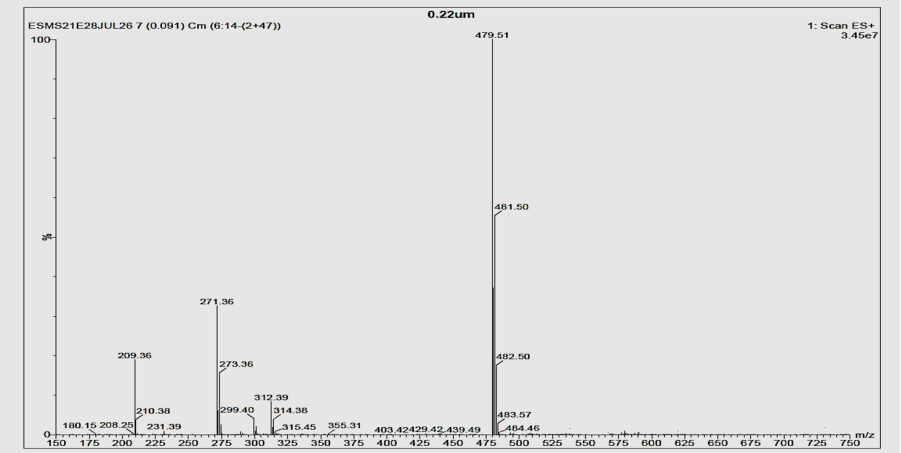

Fig. 3. HRMS of complex one

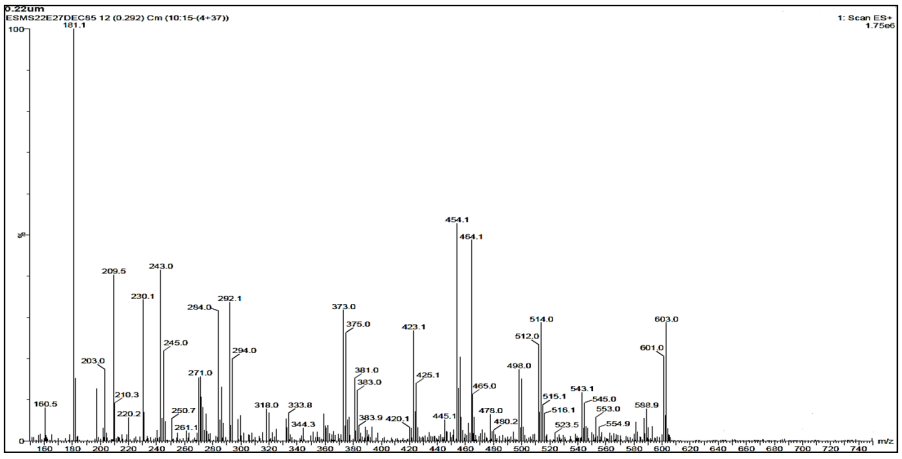

Fig. 4. HRMS of complex two

3.5. Computational results

3.5.1. Optimized structures and frontier molecular orbitals

The optimised structure of HL is represented in Figure 5a. The optimised structures of copper complexes are shown in Figure 5b and 5c. Theoretical calculations were performed on the optimised geometries of HL and complexes. The bond lengths in the optimised structure of HL are C=N 1.292 Å, C=C 1.35 Å to 1.399 Å, C-C 1.401 Å to 1.415 Å, C-O 1.371 Å, and C-Br 1.893 Å. The bond lengths in optimised structures matched the previously reported values of bond lengths.[43] In the optimized structure of complex one, Cu-N bond lengths are 1.988 Å, 2.062 Å, and Cu-O bond lengths are 1.981 Å, 2.004 Å, and for complex two, Cu-N bond lengths are 2.023 Å, 2.038 Å, 2.052 Å, Cu-Br bond length is 2.426 Å, and Cu-O bond length is 1.914 Å. **The bond lengths in optimised structures of** complexes matched the previously reported values of bond lengths. Thus, the optimized structures of HL and its complexes represent the geometry with the minimum energy and maximum stability. FMOs of HL and complexes are shown in Figure 6. The copper complexes have a lower HOMO-LUMO energy gap compared to HL. The reduction of the energy gap between HOMO and LUMO after complexation with the metal ion indicates the possibility of charge transfer in the complexes.[44] Theoretical calculated quantum chemical parameters of HL and copper complexes are given in Table 1. The chemical softness (S) and chemical hardness (η) values showed that complex two is more reactive and less stable compared to complex one [45].

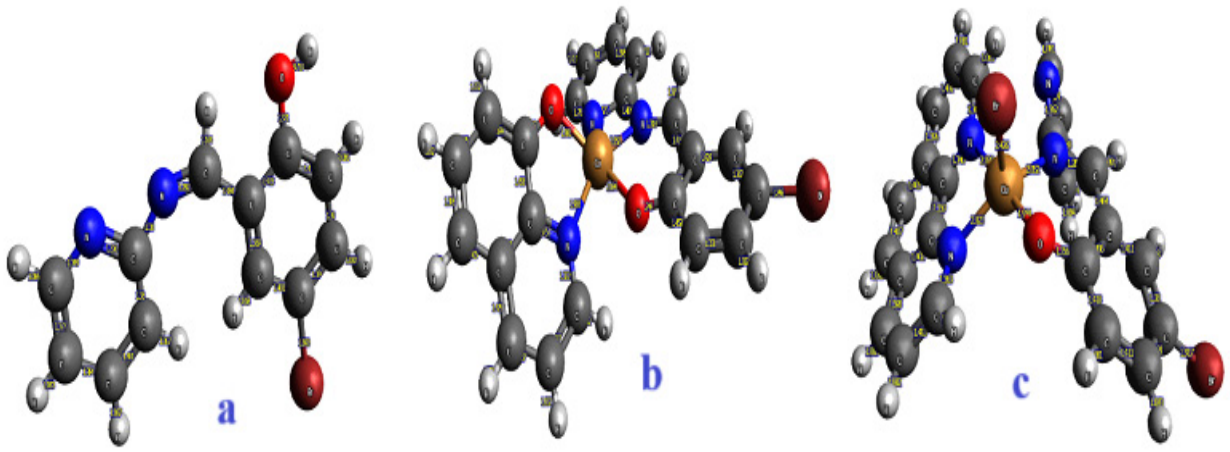

Fig. 5. Optimized geometry of **a**) HL, **b**) complex one, **c**) complex two

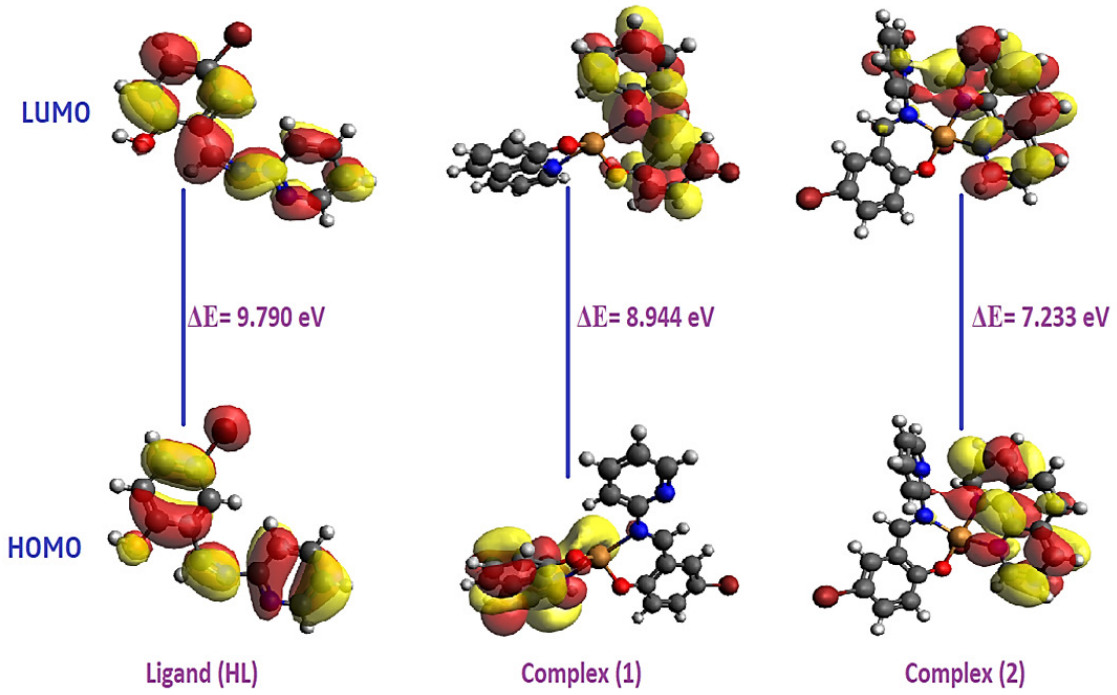

Fig. 6. FMOs of HL and complexes

Table 1. Theoretically calculated quantum chemical parameters of HL and complexes

Quantum parameters	Ligand HL	Complex one	Complex two
E_{HOMO} (eV)	-8.519	-7.496	-6.791
E_{LUMO} (eV)	1.271	1.448	0.442
E_{GAP1} (eV)	9.790	8.944	7.233
Ionization Energy (I)	8.519	7.496	6.791
Electron Affinity (A)	-1.271	-1.448	-0.442
Electronegativity (χ)	3.624	3.024	3.174
Chemical Potential (μ)	-3.624	-3.024	-3.174
Chemical Hardness (η)	4.895	4.472	3.616
Chemical Softness (S)	0.204	0.224	0.276
Electrophilicity Index (ω)	1.341	1.022	1.393

3.5.2.Electron density map

Localized Orbital Locator (LOL) and Electron Localization Function (ELF) maps are utilized to classify covalent bond analysis and charge shifts within the bonds. These maps are designed in the range of 0–1.0, where the region from 0.5-1.0 represents the bonding and non-bonding localized electrons, whereas the region below 0.5 means the delocalization of electrons [46]. LOL and ELF maps of HL are depicted in Figure 7. In LOL maps, the values are less than 0.5 for aromatic ring structure, and the electrons are delocalized in the

rings. A similar pattern of delocalization is observed in the ELF plot, with values less than 0.5, which is represented by green coloration on the aromatic ring. The electron density maps (LOL & ELF) of copper complexes are shown in Figure 8a and 8b.

The electron density maps show the green colouration on ligands bonded to the central metal ion in the complexes. This indicates the delocalization of the π-electrons and the possibility of MLCT in the complexes [47].

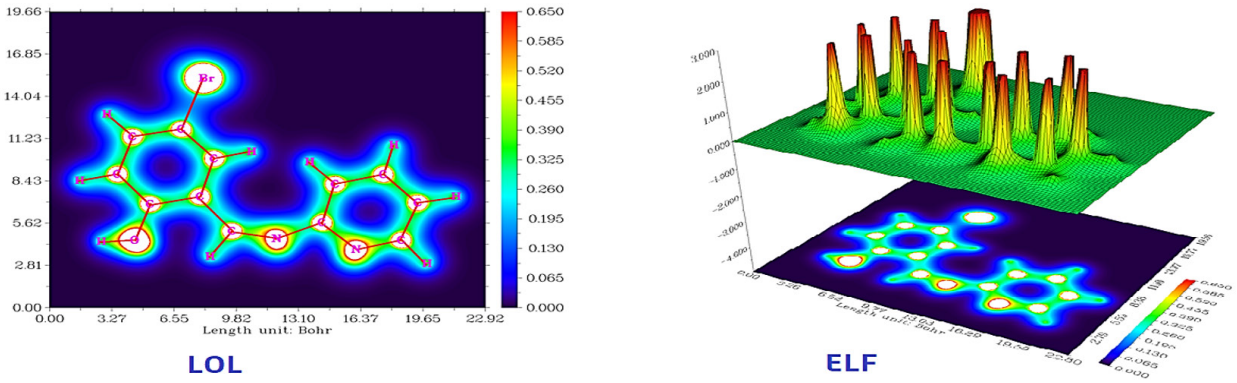

Fig. 7. LOL and ELF maps of ligand HL

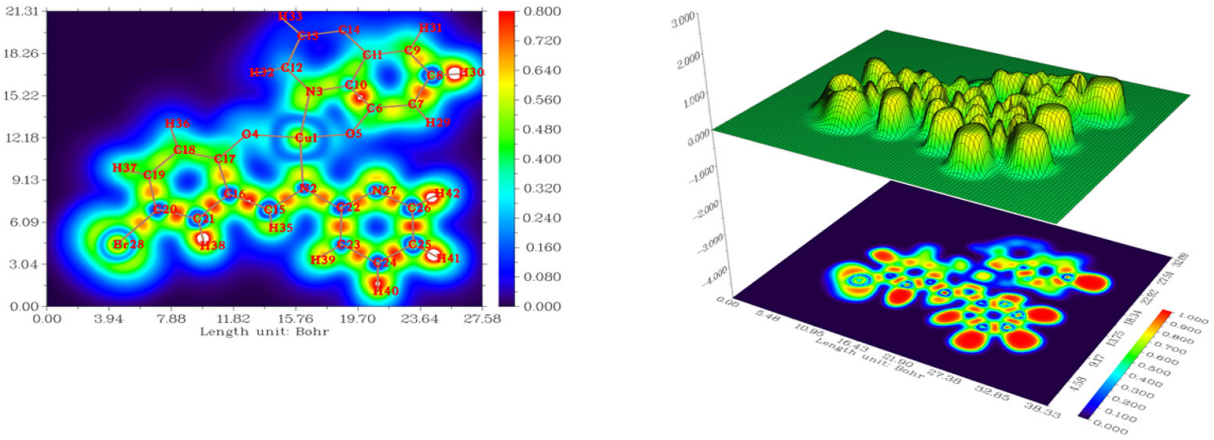

Fig. 8a. LOL and ELF maps of complex one

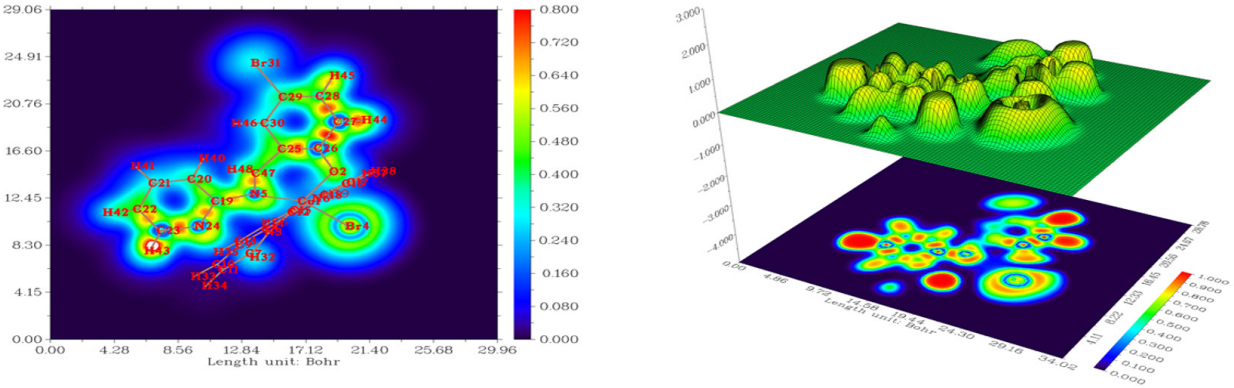

Fig. 8b. LOL and ELF maps of complex two

3.5.3. Computational IR Spectra

Theoretical calculated IR spectra of HL and complexes are shown in Figures 9a -c. Ligand (HL) has a CS point group with 69 normal vibrational modes, complex one has a C1 point group with 120 normal vibrational modes, and complex two has a C_1 point group with 138 normal vibrational modes. The selected calculated IR vibrational frequencies of HL are given in Table 2a, and values for copper complexes are shown in Tables 2b and 2c. The IR spectra exhibit only positive modes of vibration for HL and its complexes [48]. The negative imaginary mode of vibrations is absent in theoretical IR calculations for HL and its complexes, indicating that the stationary points correspond to minima of the potential energy surfaces in the optimized structure. In HL, aromatic C–H in-plane bending vibrations occur in the region 1250.8–1154.3 cm^{-1}, and C–H out-of-plane bending vibrations appear in the region 968.9–600 cm^{-1}. The stretching vibrations ν_s(C=C) and ν_s(C=N) of heterocyclic aromatic rings are observed, particularly in the regions 1400-1600 cm^{-1}. These values closely match the experimental values, where νs(C=C) is 1462.18 cm^{-1} and νs(C=N) is 1587.57 cm^{-1}. The stretching vibrations ν_s(C=N) of the imine bond occurred at 1627.4 cm^{-1}, which is very close to the experimentally obtained value (1610.73 cm^{-1} [49]. In the HL, the C-O vibrational mode of the aromatic ring appeared at 1192.2 cm^{-1} (experimental 1181.66 cm^{-1}). The C-O vibrational mode in complex one is at 1289.7 cm^{-1}(experimental 1295.42 cm^{-1}) and in complex two is at 1298.9 cm^{-1}(experimental 1250.82 cm^{-1}). Complexes have higher C-O stretching values than the ligand, and the same pattern is observed in experimental IR analysis. Similarly, imine bond C=N vibrational frequencies of complex (1) is 1532.1 cm^{-1} (experimental 1578.69 cm^{-1}) and complex (2) is 1569.2 cm^{-1} (experimental 1559.72 cm^{-1}). The vibrational frequencies of the imine bonds in the complexes are within the expected range. Furthermore, to verify the accuracy of the theoretical calculations, the Pearson correlation coefficient (r) and *P-value* were calculated for the IR results. The comparative experimental and theoretical calculated modes of vibration in the HL are given in Table 3a. The correlation coefficient (r) is 0.994, and the P-value is 0.000 for the HL. The correlation coefficient (r) is 0.995 for complex one and 0.987 for complex two, and the P-value is 0.000 for both complexes (Tables 3b and 3c). The statistical results showed that the theoretical results are comparable to the experimental results. The correlation coefficient (r) and *P-value* indicated that the selected level of theory is appropriate for theoretical calculations.

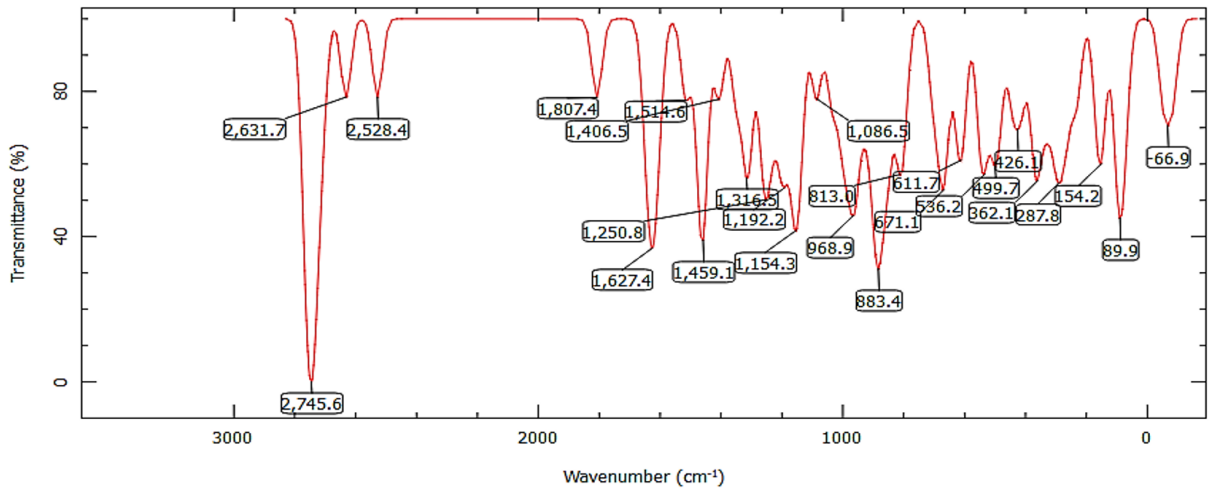

Fig. 9a. Computational IR spectra of ligand (HL)

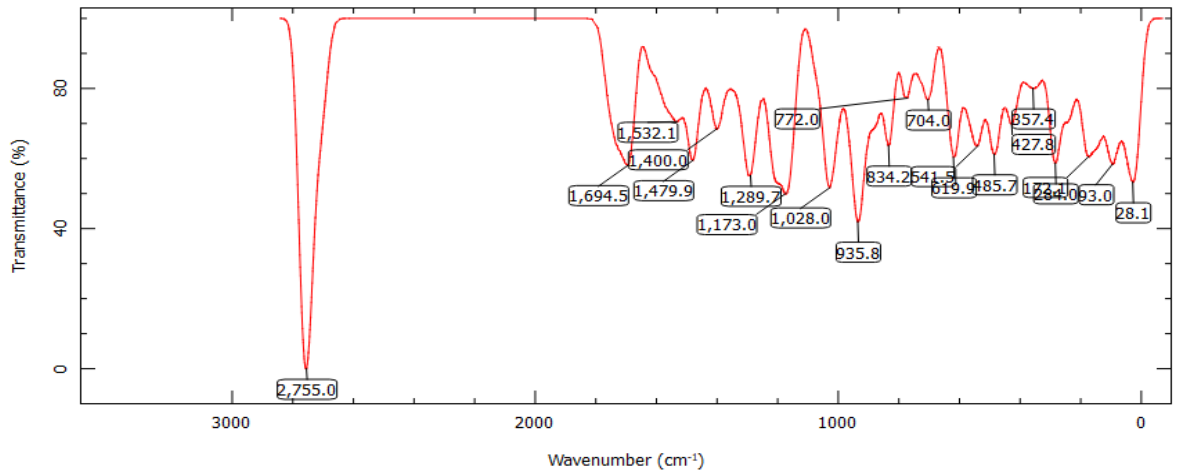

Fig. 9b. Computational IR spectra of complex one

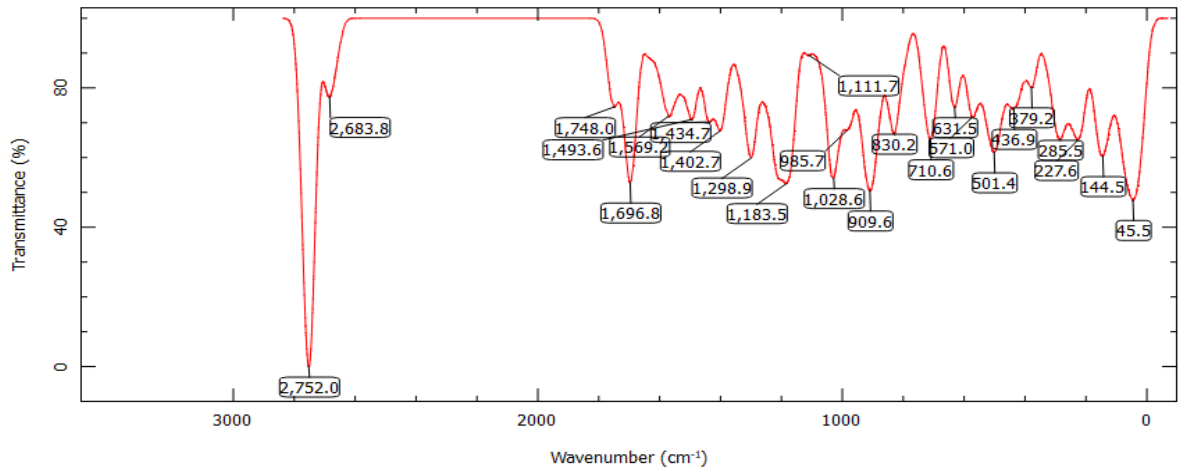

Fig. 9c. Computational IR spectra of complex two

Table 2a. The calculated IR wavenumbers (cm^{-1}) with their relative intensities of ligand HL

Mode	Frequency(cm^{-1})	Force Constant	Assignments
24	671.1	0.9058	τ CCCC + τ HCCC
27	813.0	0.2091	τ CCCC + τ HCCC + τ NCCC
31	883.4	0.3378	γ NCCC+ τ CCCC
35	968.9	0.6003	τ HCCC + γCCCC + τ CCCC
39	1086.5	0.6371	ν_b CCC
42	1192.2	0.3704	ν_sCO
46	1250.8	0.2276	ν_s CN + ν_s CH+ ν_b CO
49	1316.5	0.4805	ν_s CC + ν_s CN
51	1406.5	0.6136	ν_s CC+ ν_s CH
53	1459.1	1.7836	ν_s CC
58	1627.4	2.0449	ν_s CN
63	2745.6	1.7783	ν_{as} CH

[ν_s: symmetric stretching; ν_{as}: asymmetric stretching; ν_b: bending; τ: torsional motion; γ: out-of-plane motion]

Table 2b. The calculated IR wavenumbers (cm^{-1}) with their relative intensities of the complex one

Mode	Frequency(cm^{-1})	Force Constant	Assignments
41	619.9	0.4874	τ CCCC + τ HCCC
44	704.0	0.5621	τ CCCC + τ HCCC + τ NCCC
46	772.0	0.6860	γ NCCC+ τ CCCC
50	834.2	0.3991	τ HCCC + γCCCC + τ CCCC
56	935.8	0.4530	τ HCCC+ γNCCC + τ CCCC
63	1028.0	0.6288	ν_b CCH+ ν_b CCC
70	1173.0	0.4249	ν_b CCC+ ν_b CCH + ν_b CCBr
74	1205.5	0.3674	ν_bNCC + ν_b HCC
80	1289.7	0.2976	ν_sCO
86	1400.0	0.8477	ν_s CC + ν_s CH
91	1479.9	1.4177	ν_s CC
95	1532.1	2.5339	ν_s CN
101	1694.5	2.8293	ν_s CN
115	2759.9	1.9721	ν_{as}CH

[ν_s: symmetric stretching; ν_{as}: asymmetric stretching; ν_b: bending; τ: torsional motion; γ: out-of-plane motion

Table 2c. The calculated IR wavenumbers (cm^{-1}) with their relative intensities of the complex two

Mode	Frequency(cm^{-1})	Force Constant	Assignments
48	631.5	0.3954	τ CCCC + τ HCCC
51	710.6	0.3139	τ CCCC + τ HCCC + τ NCCC
57	830.2	0.0545	γ HCCC+ τ CCCC
69	985.7	0.2197	τ HCCC+ γNCCC+ τ CCCC
78	1111.7	0.9298	ν_b CCC+ ν_b CCH ν_b
92	1298.9	0.1458	ν_sCO
105	1493.6	1.1293	ν_s CC
110	1569.2	2.9736	ν_sCN
116	1696.8	3.1413	ν_sCN
121	1748.0	2.9957	ν_{as}CO + ν_{as}CN + ν_{as}CC
124	2683.8	3.9307	ν_{as}CH + ν_{as}CN + ν_{as}CC
133	2752.0	1.1622	ν_{as}CH

[ν_s: symmetric stretching; ν_{as}: asymmetric stretching; ν_b: bending; τ: torsional motion; γ: out-of-plane motion]

Table 3. **a**) The IR wavenumbers (cm^{-1}) of HL, **b**) complex one, **c**) complex two

S.N. **a**	Experimental wavenumber (cm^{-1})	Theoretical wavenumbers (cm^{-1})
1.	627.95	671.1
2.	817.81	813.0
3.	873.93	883.4
4.	917.62	968.9
5.	994.01	1086.5
6.	1181.66	1192.2
7.	1276.09	1250.8
8.	1345.67	1316.5
9.	1385.4	1406.5
10.	1462.18	1459.1
11.	1610.73	1627.4

S.N. **b**	Experimental wavenumber (cm^{-1})	Theoretical wavenumbers (cm^{-1})
1.	645	619.9
2.	700.05	704.0
3.	760.43	772.0
4.	824.74	834.2
5.	948.73	935.8
6.	1100.68	1028.0
7.	1149.25	1173.0
8.	1240.40	1205.5
9.	1295.42	1289.7
10.	1386.36	1400.0
11.	1469.40	1479.9
12.	1542.09	1532.1
13.	1578.69	1694.5
14.	2917.55	2759.9

S.N. **c**	Experimental wavenumber (cm^{-1})	Theoretical wavenumbers (cm^{-1})
1.	630.01	631.5
2.	761.62	710.6
3.	826.32	830.2
4.	953.92	985.7
5.	1099.82	1111.7
6.	1250.82	1298.9
7.	1385.84	1493.6
8.	1542.08	1569.2
9.	1642.56	1696.8
10.	1844.03	1748.0
11.	2395.26	2683.8
12.	2920.80	2752.0

**r of experimental and theoretical wavelength = 0.99, *P*-Value = 0.000

3.5.4. Computational Electronic Spectra

The computational UV-visible spectra of HL and copper complexes are shown in Figure 10. The absorption peaks at 260.7 nm (f_{osc} 0.138826932), 282.8 nm (f_{osc} 0.164941980), and 313.8 nm (f_{osc} 0.347646555) are due to the π→ π∗ transitions in HL, and the peaks at 388.1 nm (f_{osc} 0.147941030) are due to the n→ π∗ transition. The n→ π∗ transition occurred closer to the visible region and is responsible for the characteristic colour of HL. The absorption region in computational spectra of HL is the same as observed in the experimental spectra. However, the absorption maxima values cannot be compared because, according to the Beer-Lambert law, absorption is concentration-dependent, which causes changes in the shape and position of absorption bands. In the metal complexes, the computational UV-visible spectrum of the complex one exhibits peaks with absorption maxima at 812.75 nm (fosc 0.025139439, 2B1g→2Eg) and 610.1 nm (fosc 0.051543107, 2B1g→2A1g), corresponding to the d-d transitions, which require less energy for excitation. The charge transfer absorption band maxima in complex one is at 414.4 nm (f_{osc} 0.050521191) [50]. Similarly, complex two has peaks due to d-d transitions with absorption maxima at 674.1 nm (f_{osc} 0.012868192, $^2B_1 \rightarrow {}^2A_1$), 642.1 nm ($f_{osc}$ 0.026937661, $^2B_1 \rightarrow {}^2B_2$), and 600.0 nm ($f_{osc}$ 0.021139092, $^2B_1 \rightarrow {}^2E$). The charge transfer band in complex two is observed at 465.5 nm (fosc = 0.011944701) and 475.8 nm (fosc = 0.011818970).

3.5.5. Computational HRMS analysis

The Predicted Ligand HRMS spectrum obtained at 20V. The fragmentation pattern of HL is depicted in Figure 11. The predicted HRMS spectra of HL followed the same fragmentation pattern as shown in

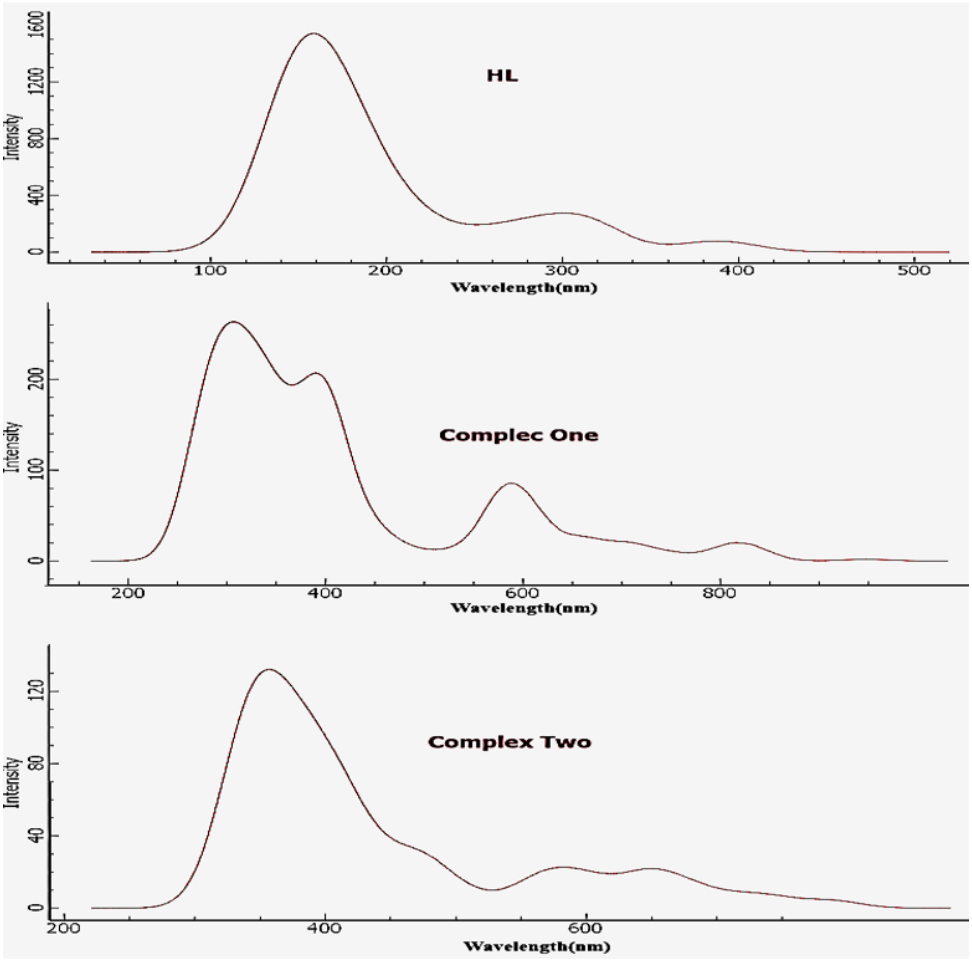

Fig. 10. Computational electronic spectra of HL, complex one, and two

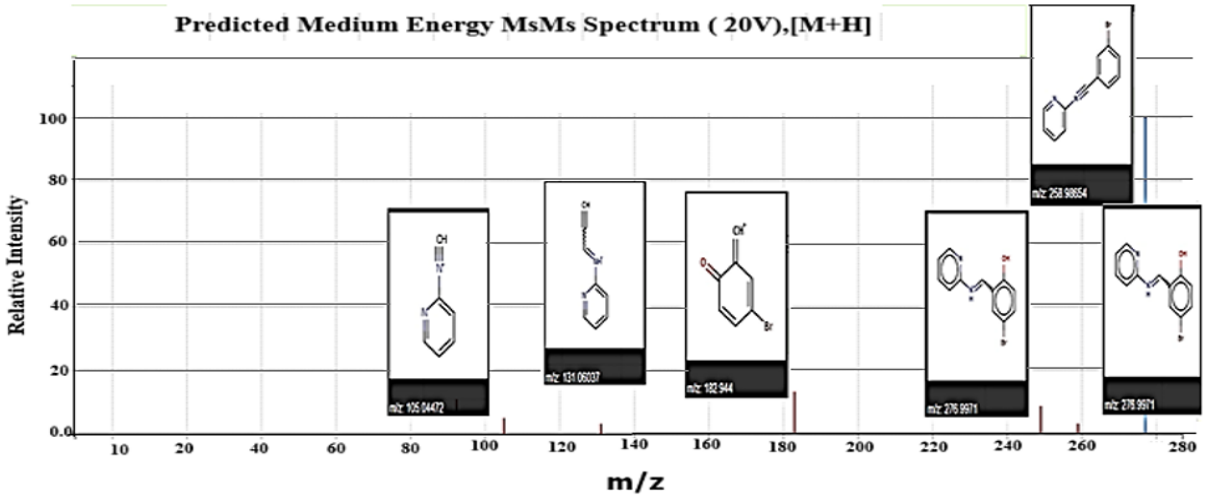

Fig. 11. Predicted mass spectrum of ligand (HL)

the experimental spectra, with the highest intensity peak corresponding to the molecular ion. The isotopic abundances of elements in coordination compounds pose a significant challenge to computational HRMS investigations, as they can form broad clusters through multiple fragmentation pathways, resulting in complex spectral patterns. So, the computational HRMS for complexes could not be predicted by the software [51].

3.5.6.Molecular docking results

Molecular docking was performed at the active site of acetylcholinesterase (AChE) from Drosophila Melanogaster (fruit flies). Docking was also performed with the already known pyridine-based insecticide acetamiprid. The interaction at the binding site of AChE with HL is shown in Figure 12, and with acetamiprid is shown in Figure 13. The binding energy value for HL is -8.2 kcal mol^{-1}, and for acetamiprid is -6.8 kcal mol^{-1}. The interaction at the binding site of AChE with complex one is shown in Figure 14, and with complex two is shown in Figure 15. The binding energy value for complex one is -7.9 kcal mol^{-1}, and complex two is -6.2 kcal mol^{-1}. The negative values of the binding energy indicated that HL, acetamiprid, and the complexes have a favourable binding with the AChE enzyme [52]. The meaningful non-covalent interactions and their corresponding distances are tabulated in Table 4. The HL has a stacking interaction with HIS:480 amino acid, which is one of the amino acids of the catalytic triad (Glu367/His480/Ser238). Besides this, HL has interaction with the peripheral residue TYR:83 of the choline-binding pocket (Trp83). These interactions assure the binding of HL with the active site of AChE. The Hydrogen bond interaction played a vital role in holding HL in the binding site of the AChE. The HL formed two hydrogen bonds, one with TYR:71 (1.85 Å) and another with GLY:150 (2.37 Å). The distances of hydrogen bonds are in the specified range of real docking (≤ 3.5 Å) [53]. Acetamiprid and HL interact with the identical amino acid residues in the target site of docking. Acetamiprid formed hydrogen bonds with HIS:480 (2.28 Å). These interactions showed that HL is a potential candidate for insecticidal properties. The complex one has stacking interaction with the peripheral site residue TYR:321 and ionic interactions with ASP:375. The copper complexes have a larger surface area compared to the ligands. The size of the binding pocket in the catalytic triad site of AChE is small, so the copper complexes did not fit at the active site and interacted with the peripheral site residues. The complex two has ionic interactions with LYS:278 and LYS:403, as well as hydrophobic interactions with LYS:403 and PRO:270. The binding energy values also suggested that HL has a higher binding potential with acetylcholinesterase (AChE) compared to copper complexes and acetamiprid.

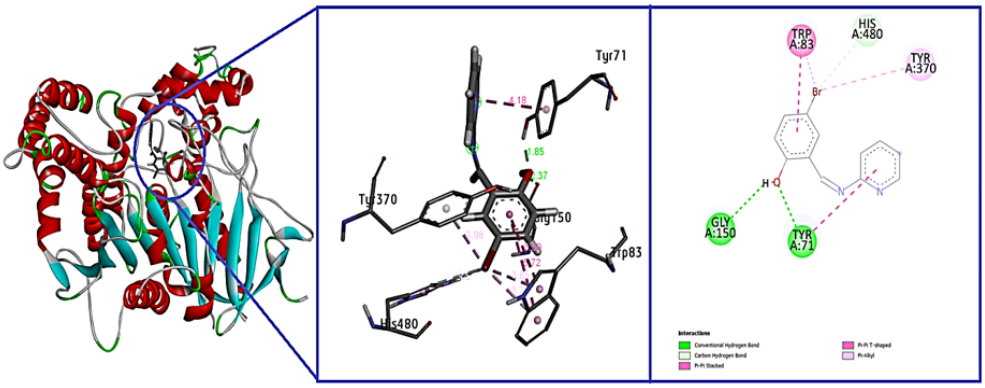

Fig.12. Interaction of HL with the active site of acetylcholinesterase (AChE) from Drosophila melanogaster (fruit flies)

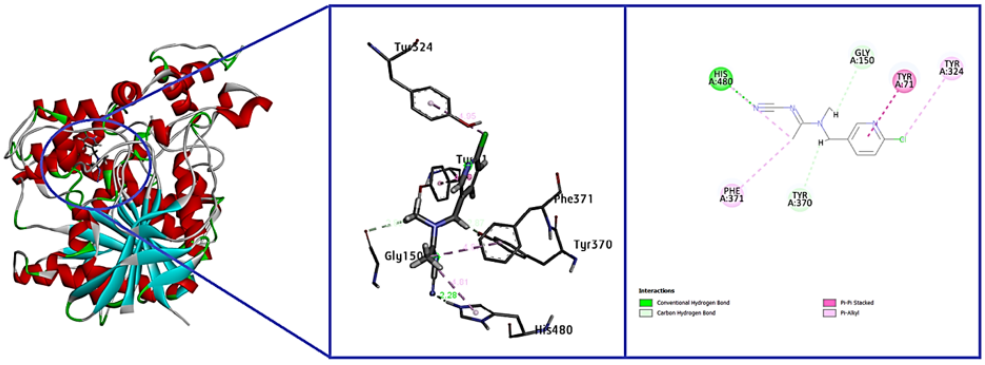

Fig. 13. Interaction of acetamiprid with the active site of acetylcholinesterase (AChE) from Drosophila melanogaster (fruit flies)

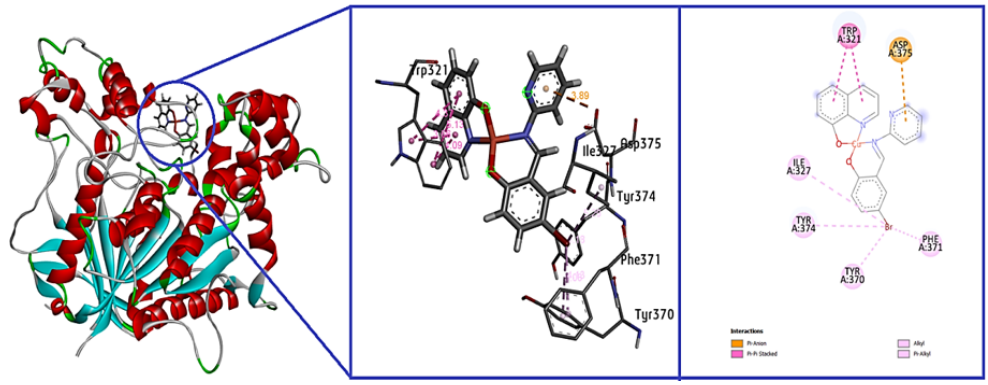

Fig. 14. Interaction of complex one with the acetylcholinesterase (AChE)

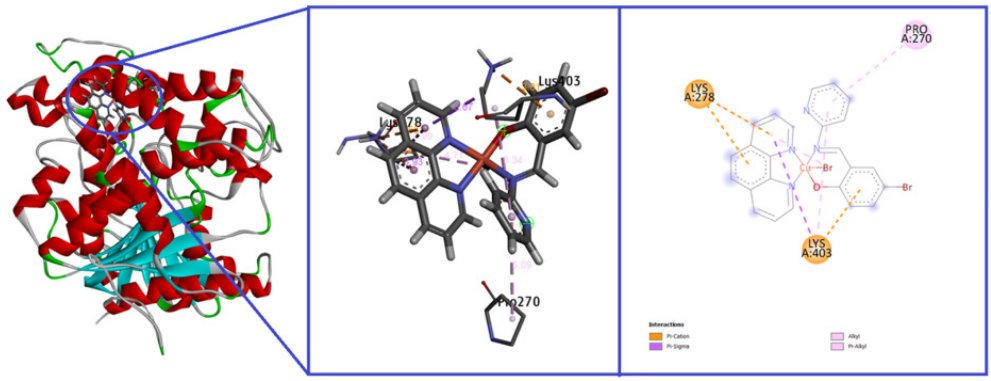

Fig. 15. Interaction of complex two with the acetylcholinesterase (AChE) from Drosophila Melanogaster (fruit flies)

Table 4. Intermolecular interactions at the binding site of AChE with HL and copper complexes.

Molecules	Binding energy (kcal mol^{-1})	RSMD (ub/lb)	Hydrogen bond/ Ionic interactions	Hydrophobic Interactions
Acetamiprid	-6.8	0/0	HIS:480 (2.28 Å) GLY:150 (2.80 Å) TYR:370 (2.87Å)	TYR:324 (4.95 Å) PHE:371 (4.87 Å) TYR: 71 (4.86 Å)
Ligand (HL)	-8.2	0/0	TYR:71(1.85 Å) GLY:150 (2.37 Å)	TYR:370 (3.98 Å) TYR: 83 (3.72 Å) TYR: 71 (4.18 Å) HIS:480 (4.50 Å) TYR:370 (3.98 Å)
Complex one	-7.9	0/0	ASP:375 (3.89 Å)	PHE:371 (4.13 Å) TYR:374 (5.18 Å) TRP:370 (5.08 Å) TYR:321 (3.66 Å) ILE: 327 (5.29 Å)
Complex two	-6.2	0/0	LYS:278 (3.53 Å) LYS:403 (3.81 Å)	LYS:403 (3.67 Å) PRO:270 (5.09 Å)

ub/lb: Indicates the upper and lower bounds of the RMSD calculation

3.5.7.Physico-chemical Parameters and Toxicity Results

The physicochemical properties and toxicity of HL and its metal complexes are obtained using the in-silico method and are listed in Table 5. The log $P_{o/w}$ (the octanol-water partition coefficient) for HL and copper complexes is in the acceptable range (-0.4–5.6). The log $P_{o/w}$ represents the aqueous solubility, which measures the tendency of the molecule to penetrate the biological membrane. The TPSA (Total polar surface area) for HL and copper complexes is in the acceptable ranges (≤ 140) [54]. The toxicological study of the HL and copper complexes showed that HL and both complexes are non-AMES toxic and non-carcinogens. HL and copper complexes exhibit low toxicity to honeybees but high toxicity to Tetrahymena pyriformis. HL has low fish toxicity, but copper complexes have higher fish toxicity. The LD_{50} of acute toxicity in the rat is the amount of dose that causes 50% mortality within 24 hours of administration. The lethal dose (LD_{50}) value for HL is 2.5014 mol Kg^{-1}, for complex (1) is 2.6031 mol Kg^{-1}, and for complex two is 2.6659 mol Kg^{-1}. HL and complexes are not readily biodegradable.

3.5.8. Insecticidal Bio-efficacy and Toxicity (in vitro)

The 20 mg L^{-1} (0.024 g L^{-1} for HL, 0.022 g L^{-1} for complex one (1), and 0.026 g L^{-1} for complex two) stock solutions of HL and complexes were diluted to prepare 500 mL of 10 mg L^{-1} solution. Solutions of HL and its complexes at concentrations of 50 mL of 4000 µg L^{-1}, 3000 µg L^{-1}, 2000 µg L^{-1}, 1000 µg L^{-1}, and 500 µg L^{-1} are prepared by further dilution of 20 mg L^{-1} or 10 mg L^{-1}. The five groups of Drosophila melanogaster (each containing 10 adults) were used to determine the LD_{50} value of HL. The results obtained are presented in Table 6. The LD_{50} value for HL is 1800 µg L^{-1}. Similarly, the obtained toxicological data for complex one are presented in Table 7, and those for complex two are presented in Table 8. The LD_{50} value for complex one is 2325 µg L^{-1}, and complex two (2) is 2175 µg L^{-1}. The in vitro analysis results indicate that HL and its complexes are biologically active against Drosophila melanogaster. The LD_{50} value of HL is less than that of complexes, which indicates HL is more toxic than complexes [55].

Table 5. In-silico physicochemical properties and toxicity data of HL and copper complexes

Properties	HL	Complex one	Complex two
Physicochemical			
Number of H-bond acceptors	3	3	2
Number of H-bond donors	1	0	0
Lipophilicity (Log Po/w)	2.84	2.77	2.67
Water Solubility	Soluble	Moderately soluble	Moderately soluble
Molar Refractivity	67.66	111.89	123.68
TPSA(Å2)	45.48	38.24	31.84
Aqueous solubility (LogS)	-3.4404	-4.1773	-3.9688
Toxicity			
AMES Toxicity	Non	Non	Non
Carcinogens	Non	Non	Non
Fish Toxicity	Low FHMT	High FHMT	High FHMT
Honey Bee Toxicity	Low HBT	Low HBT	Low HBT
*TPT	High TPT	High TPT	High TPT
Biodegradation (BD)	Not BD II	Not BD III	Not BD III
Acute Oral Toxicity			
Acute Toxicity (LD50, mol Kg^{-1})	2.5014	2.6031	2.6659
Fish Toxicity (pLC50, mg L^{-1})	1.3578	1.1453	1.0728
TPT (pIGC50, ug L^{-1})	1.9460	1.0663	0.9835
Drug likeness			
Lipinski	Yes	Yes	Yes
Bioavailability Score	0.55	0.55	0.55
Synthetic accessibility	2.54	4.92	5.03

***TPT:** *Tetrahymena Pyriformis Toxicity*

Table 6. In vitro toxicological data of ligand HL

Dose (μg L^{-1})	Test Number (N)	Dose Difference (a)	Dead (N)	Interval mean (b)	Product (a×b)
500	10	-----	0	---	---
1000	10	500	4	2	1000
2000	10	1000	6	5	5000
3000	10	1000	7	6.5	6500
4000	10	1000	10	9.5	9500
					22000

LD_{50} = 4000 – 22000/10 = 1800 μg L^{-1} = 1.8 mg L^{-1}

Table 7. In vitro toxicological data of complex one

Dose (µg L^{-1})	Test Number (N)	Dose Difference (a)	Dead (N)	Interval mean (b)	Product (a×b)
500	10	-----	0	---	---
1000	10	500	1	0.5	250
2000	10	1000	4	2.5	2500
3000	10	1000	7	5.5	5500
4000	10	1000	10	8.5	8500
					16750

LD_{50} = 4000 – 16750/10 = 2325 µg L^{-1} = 2.325 mg L^{-1}

Table 8. In vitro toxicological data of complex two

Dose (µg L^{-1})	Test Number (N)	Dose Difference (a)	Dead (N)	Interval mean (b)	Product (a×b)
500	10	-----	0	---	---
1000	10	500	1	0.5	250
2000	10	1000	4	3	3000
3000	10	1000	8	6	6000
4000	10	1000	10	9	9000
					18250

LD_{50} = 4000 – 18250/10 = 2175 µg L^{-1} = 2.175 mg L^{-1}

4. Conclusion

The heterocyclic-based Schiff base (HL) was synthesized by the refluxing method, and the heteroleptic complexes of HL with copper, [Cu(L)(8HQ)] complex one and [Cu(L)(phen)Br] complex two, were formed by the liquid-assisted grinding (LAG) method. The chemical softness (S) and chemical hardness (η) values revealed that complex two is more reactive and less stable compared to complex one. For IR spectra, the correlation coefficient (r) is closer to one, and the P value is 0.000 for the HL and copper complexes. The correlation coefficient (r) and P value indicated that the selected level of theory is appropriate for the theoretical calculations. The negative values of the binding energy showed that the HL and copper complexes have favourable binding with the AChE enzyme of Drosophila melanogaster (fruit flies). Acetamiprid and HL have an interaction with identical amino acid residues in the target site of docking. The log $P_{o/w}$ (the octanol-water partition coefficient) for the HL and copper complexes is in the acceptable range. The HL and copper complexes exhibit low toxicity to honey bees but high toxicity to Tetrahymena pyriformis. The HL has low fish toxicity, but the copper complexes have higher fish toxicity. In vitro analysis results indicate that the HL and complexes are biologically active against Drosophila melanogaster. Thus, the findings of the present study elucidate the insecticidal properties of pyridine-based Schiff base (HL) and its Cu(II) complexes, prompting the insecticidal design community to develop new insecticides with novel modes of action.

5. Acknowledgments

The authors are thankful to CDRI, Lucknow, U.P. (India) for providing the spectral facilities for UV-visible and IR and mass spectrometry. We are thankful to Department of Entomology, B. R. D. P. G. College, Deoria- Uttar Pradesh for providing the culture of Drosophila melanogaster. We are thankful to Mr. Mritunjay Maurya, Agriculture Officer, Department of Agriculture, Uttar Pradesh-India, for his guidance and help for in-vitro analysis. Drosophila melanogaster is not listed

as an endangered or threatened species in India's official Red Data Book. It is a common and widely distributed species with a large global population and a well-established model for research in India. Therefore, there are as such no ethical codes to conduct research on Drosophila melanogaster in India.

6. References

[1] M.A. Neelakantan, M. Esakkiammal, S.S. Mariappan, J. Dharmaraja, T. Jeyakumar, Synthesis, characterization and biocidal activities of some Schiff base metal complexes, Indian J. Pharm. Sci., 72 (2010) 216–222. https:// doi.org/ 10.4103/0250-474X .65015

[2] R. Ashouri, S. A. Hajiseyed Mirzahosseini, N. Mansouri, Synthesis of carbon quantum dots from olive stones for efficient adsorption of benzene from the ambient air, J. Nanostruct., 11 (2021) 480-497. https://doi.org/10.22052/JNS.2021.03.007

[3] M. Arjomandi, A review: analytical methods for heavy metals determination in environment and human samples, Anal. Methods Environ. Chem. J., 2 (2019) 97-126. https://doi.org/10.24200/amecj.v2.i03.73

[4] L. John, R. S. Joseyphus, I. H. Joe, Biomedical application studies of Schiff base metal complexes containing pyridine moiety: Molecular docking and a DFT approach, SN Appl. Sci., 2 (2020) 500. https://doi.org/10.1007/s42452-020-2274-6

[5] A. P. Matos, A. L. F. Sarria, A. C. Volante, A. R. Bernardo, G. O. S. Cunha, J. B. Fernandes, P. C. Vieira, M. F. D. G. F. da Silva, Potential insecticidal activity of aminonaphthoquinone Mannich bases derived from lawsone and their copper (II) complex derivatives, Zeitschrift fur Naturforschung C, J. biosci., 76 (2020) 111–115. https://doi.org/10.1515/znc-2020-0115

[6] N. Raman, J. Joseph, A. S. Velan, C. Pothiraj, Antifungal activities of biorelevant complexes of copper(II) with biosensitive macrocyclic ligands, Mycobiology, 34 (2006) 214–218. https://doi.org/10.4489/MYCO.2006.34.4.214

[7] D. Kudasova, B. Mutaliyeva, K. Vlahoviček-Kahlina, S. Jurić, M. Marijan, S. V. Khalus, A. V. Prosyanik, S. Šegota, N. Španić, M. Vinceković, Encapsulation of synthesized plant growth regulator based on copper(II) complex in chitosan/alginate microcapsules, Int. J. Mol. Sci., 22 (2021) 2663. https://doi.org/10.3390/ijms22052663

[8] E. Bursal, F. Turkan, K. Buldurun, N. Turan, A. Aras, N. Çolak, M. Murahari, M. C. Yergeri, Transition metal complexes of a multidentate Schiff base ligand containing pyridine: Synthesis, characterization, enzyme inhibitions, antioxidant properties, and molecular docking studies, BioMetals, 34 (2021) 393–406. https://doi.org/10.1007/s10534-021-00287-z

[9] N. S. Millar, I. Denholm, Nicotinic acetylcholine receptors: Targets for commercially important insecticides, Invert. Neurosci., 7 (2007) 53–66. https://doi.org/10.1007/s10158-006-0040-0

[10] J. E. Casida, G. B. Quistad, Golden age of insecticide research: past, present and future, Ann. Rev. Entomol., 43 (1998) 1-16. https://doi.org/10.1146/annurev.ento.43.1.1

[11] M. Pohanka, Acetylcholinesterase inhibitors: A patent review (2008 – present), Expert Opin. Ther. Pat., 22 (2012) 871–886. https://doi.org/10.1517/13543776.2012.701620.

[12] J. Győri, A. Farkas, O. Stolyar, A. Székács, M. Mörtl, A. Vehovszky, Inhibitory effects of four neonicotinoid active ingredients on acetylcholine esterase activity, Acta Biol. Hung., 68 (2017) 345–357. https://doi.org/10.1556/018.68.2017.4.1

[13] J. Somers, J. Nguyen, C. Lumb, P. Batterham, T. Perry, In vivo functional analysis of the Drosophila melanogaster nicotinic acetylcholine receptor Dα6 using the insecticide Spinosad, Insect Biochem. Mol. Biol., 64 (2005) 116–127. https://doi.org/10.1016/j.ibmb.2015.01.018

[14] H. M. Abd El-Lateef, M. M. Khalaf, M. Gouda, M. Kandeel, A. A. Amer, A. A. Abdelhamid, A. M. Drar, M. A. Gad, Functionalized pyridines: Synthesis and toxicity evaluation of potential

insecticidal agents against Aphis Craccivora, ACS Omega, 8 (2023) 29685–29692. https://doi.org/10.1021/acsomega.3c03831

[15] A.Y.Guan,C.L.Liu,X.F.Sun,Y.Xie,M.A.Wang, Discovery of pyridine-based agrochemicals by using intermediate derivatization methods, Recent Dev. Agrochem., 24 (2016) 342–353. https:// doi.org/ 10.1016/ j.bmc.2015.09.031

[16] J.P. Jansen, T. Defrance, A. M. Warnier, Side effects of flonicamide and pymetrozine on five aphid natural enemy species, BioControl., 56 (2011) 759–770. https://doi.org/10.1007/s10526-011-9342-1

[17] V. V. Zakharychev, A. V. Kuzenkov, A. M. Martsynkevich, Good pyridine hunting: A biomimic compound, a modifier and a unique pharmacophore in agrochemicals, Chem. Heterocycl. Compd., 56 (2020) 1491–1516. https://doi.org/10.1007/s10593-020-02843-w

[18] A. Wróblewska, G. Lauriol, G. Mlostoń, X. Bantreil, F. Lamaty, Expedient synthesis of NOxy-heterocyclic carbenes (NOHC) ligands and metal complexes using mechanochemistry, J. Organomet. Chem., 949 (2021) 121914. https://doi.org/10.1016/j.jorganchem.2021.121914

[19] T. Friščić, C. Mottillo, H. M. Titi, Mechanochemistryforsynthesis, Angew. Chem. Int. Ed. Engl., 59 (2020) 1018–1029. https://doi.org/ 10.1002/ anie. 201906755

[20] V. K. Singh, A. Chamberlain-Clay, H. C. Ong, F. León, G. Hum, M. Y. Par, P. Daley-Dee, F. García, Multigram mechanochemical synthesis of a salophen complex: A comparative analysis, ACS Sustain. Chem. Eng., 9 (2021) 1152–1160. https://doi.org/10.1021/acssuschemeng.0c06374

[21] A. P. Amrute, J. De Bellis, M. Felderhoff, F. Schüth, Mechanochemical synthesis of catalytic materials, Chem. Eur. J., 27 (2021) 6819–6847. https://doi.org/10.1002/chem.202004583

[22] F. Neese, The ORCA program system, WIREs Comput. Mol. Sci., 2 (2021) 73–78. https://doi.org/10.1002/wcms.81

[23] A. G. Martynov, J. Mack, A. K. May, T. Nyokong, Y. G. Gorbunova, A. Y. Tsivadze, Methodological survey of simplified TD-DFT methods for fast and accurate interpretation of UV–Vis–NIR spectra of phthalocyanines, ACS Omega, 4 (2019) 7265–7284. https://doi.org/10.1021/acsomega.8b03500

[24] M. Mohammadi Asl, N. Mansouri, S. A. R. Haji Seyed Mirzahosseini, F. Atabi, Simultaneity comparative evaluation of toluene removal from the air by adsorption and UV semi-degradation-based adsorption procedure, Int. J. Environ. Sci. Technol., 21 (2024) 6677-6694. https://doi.org/10.1007/s13762-024-055

[25] M. M. Asl, F. Atabi, Functionalized graphene oxide with bismuth and titanium oxide nanoparticles for efficiently removing formaldehyde from the air by photocatalytic degradation–adsorption process, J. Anal. Test., 7 (2023) 444-458. https://doi.org/10.1007/s41664-023-00272-0

[26] R. De Levie, Two linear correlation coefficients, J. Chem. Educ., 80 (2003) 1030. https://doi.org/10.1021/ed080p1030

[27] O. Trott, A. J. Olson, AutoDock Vina: Improving the speed and accuracy of docking with a new scoring function, efficient optimization, and multithreading, J. Comput. Chem., 31 (2010) 455–461. https://doi.org/10.1002/jcc.21334

[28] J. Rakhtshah, N. Esmaeil, A rapid extraction of toxic styrene from water and wastewater samples based on hydroxyethyl methylimidazolium tetrafluoroborate immobilized on MWCNTs by ultra-assisted dispersive cyclic conjugation-micro-solid phase extraction, Microchem. J., 170 (2021) 106759. https://doi.org/10.1016/j.microc.2021.106759

[29] F. Nachon, T. L. Rosenberry, I. Silman, J. L. Sussman, A second look at the crystal structures of *Drosophila melanogaster* acetylcholinesterase in complex with tacrine derivatives provides insights concerning catalytic intermediates and the design of specific insecticides, Molecules, 25 (2025) 1198. https://doi.org/10.3390/molecules25051198

[30] D.S. Biovia, Discovery Studio Modeling Environment, Dassault Syst. Release, San Diego, CA, USA, 2015. https:// www.scirp.org/ reference/ referencespapers? referenceid= 2450411

[31] A. Daina, O. Michielin, V. Zoete, SwissADME: a free web tool to evaluate pharmacokinetics, drug-likeness and medicinal chemistry friendliness of small molecules, Sci. Rep., 7 (2017) 42717, https://doi.org/10.1038/srep42717

[32] E. Chinedu, D. Arome, F. S. Ameh, A new method for determining acute toxicity in animal models, Toxicol. Int., 20 (2013) 224–226. https://doi.org/10.4103/0971-6580.121674

[33] E. Ermiş, A. Aydın, H. Ünver, S. Sezen, M. B. Mutlu, Microwave-assisted synthesis, experimental and theoretical characterization and antibacterial activity screening of novel azomethine compounds containing thiophene and aminophenol functionality, Spectrochim. Acta A Mol. Biomol. Spectrosc., 243 (2020) 118761. https://doi.org/10.1016/j.saa.2020.118761

[34] J. L. Do, T. Friščić, Mechanochemistry: A force of synthesis, ACS Cent. Sci., 3 (2017) 13–19. https://doi.org/10.1021/acscentsci.6b00277

[35] A. Carreño, L. Rodríguez, D. Páez-Hernández, R. Martin-Trasanco, C. Zúñiga, D. P. Oyarzún, M. Gacitúa, E. Schott, R. Arratia-Pérez, J. A. Fuentes, Two new fluorinated phenol derivatives pyridine Schiff bases: Synthesis, spectral, theoretical characterization, inclusion in epichlorohydrin-β-cyclodextrin polymer, and antifungal effect, Front. Chem., 6 (2018) 312. https://doi.org/10.3389/fchem.2018.00312

[36] A. Faghihi-Zarandi, J. Rakhtshah, B. B. Yarahmadi, A rapid removal of xylene vapor from environmental air based on bismuth oxide coupled to heterogeneous graphene/graphene oxide by UV photo-catalectic degradation-adsorption procedure, J. Environ. Chem. Eng., 8 (2020) 104193. https://doi.org/10.1016/j.jece.2020.104193

[37] G. A. A. Al-Hazmi, K. S. Abou-Melha, N. M. El-Metwaly, I. Althagafi, F. Shaaban, R. Zaky, Green synthesis approach for Fe (III), Cu (II), Zn (II) and Ni (II)-Schiff base complexes, spectral, conformational, MOE-docking and biological studies, Appl. Organomet. Chem., 34 (2020) e5403. https://doi.org/10.1002/aoc.5403

[38] B. J. Rudresha, B. Ramachandra Bhat, H. C. Sampath Kumar, K. I. Shiva Kumar, K. Safakath, R. Philip, Synthesis, characterization and third-order nonlinear optical studies of copper complexes containing 1,10-phenanthroline-5,6-dione and triphenylphosphine ligands, Synth. Met., 161 (2011) 535–539. https://doi.org/10.1016/j.synthmet.2010.12.006

[39] H. A. Patwardhan, S. Gopinathan, C. Gopinathan, Chelated titanium(VI) compounds of salicylaldazines, Indian J. Chem., 16 (1978) 224-227. https://or.niscpr.res.in/index.php/IJC

[40] R. A. Palmer, T. S. Piper, 2,2'-Bipyridine complexes. I. polarized crystal spectra of tris (2,2'-bipyridine) copper(II), nickel(II), cobalt(II), iron(II), and ruthenium(II),Inorg.Chem., 5 (1966) 864–878. https://doi.org/10.1021/ic50039a034

[41] S. Altürk, D. Avcı, A. Başoğlu, Ö. Tamer, Y. Atalay, N. Dege, Copper (II) complex with 6-methylpyridine-2-carboxyclic acid: Experimental and computational study on the XRD, FT-IR and UV–Vis spectra, refractive index, band gap and NLO parameters, Spectrochim. Acta A Mol. Biomol. Spectrosc., 190 (2018) 220-230. https://doi.org/10.1016/j.saa.2017.09.041

[42] T. L. Yusuf, S. D. Oladipo, S. Zamisa, H. M. Kumalo, I. A. Lawal, M. M. Lawal, N. Mabuba, Design of new Schiff-base copper(II) complexes: Synthesis, crystal structures, DFT study, and binding potency toward cytochrome P450 3A4, ACS Omega, 6 (2021) 13704–13718. https://doi.org/10.1021/acsomega.1c00906

[43] M. Rbaa, A. Oubihi, H. Hajji, B. Tüzün, A. Hichar, E. H. Anouar, E. Berdimurodov, M. A. Ajana, A. Zarrouk, B. Lakhrissi, Synthesis, bioinformatics and biological evaluation of novel pyridine based on 8-hydroxyquinoline derivatives as antibacterial agents: DFT, molecular docking and ADME/T studies, J. Mol. Struct., 1244 (2021) 130934. https://doi.org/10.1016/j.molstruc.2021.130934

[44] M. Abd El Aleem Ali Ali El-Remaily, O.

Elhady, A. Abdou, D. Alhashmialameer, T. N. A. Eskander, A. M. Abu-Dief, Development of new 2-(Benzothiazol-2-Ylimino)-2,3-Dihydro-1H-imidazol-4-Ol complexes as a robust catalysts for synthesis of thiazole 6-carbonitrile derivatives supported by DFT studies, J. Mol. Struct., 1292 (2023) 136188. https://doi.org/10.1016/j.molstruc.2023.136188

[45] S. Teimoori, A. H. Hassani, M. Panahi, N. Mansouri, Rapid extraction of BTEX in water and milk samples based on functionalized MWCNTs by dispersive homogenized-micro-solid phase extraction, Food Chem., 421 (2023) 136229. https://doi.org/10.1016/j.foodchem.2023.136229

[46] S. Teimoori, A. H. Hassani, New extraction of toluene from water samples based on nano-carbon structure before determination by gas chromatography, Int. J. Environ. Sci. Technol., 20 (2023) 6589–6608. https://doi.org/10.1007/s13762-023-04906-9

[47] S. Janani, H. Rajagopal, S. Muthu, S. Aayisha, M. Raja, Molecular structure, spectroscopic (FT-IR, FT-Raman, NMR), HOMO-LUMO, chemical reactivity, AIM, ELF, LOL, and molecular docking studies on 1-benzyl-4-(N-Boc-amino)piperidine, J. Mol. Struct., 1230 (2021) 129657. https://doi.org/10.1016/j.molstruc.2020.129657

[48] R. Ashouri, N. Mansouri, Dynamic and static removal of benzene from air based on task-specific ionic liquid coated on MWCNTs by sorbent tube-headspace solid-phase extraction procedure, Int. J. Environ. Sci. Technol., 18 (2021) 2377-2390. https://doi.org/10.1007/s13762-020-02995-4

[49] S. A. Zarei, D. Khaledian, K. Akhtari, K. Hassanzadeh, Copper(II) and nickel(II) complexes of tetradentate Schiff base ligand: UV-Vis and FT-IR spectra and DFT calculation of electronic, vibrational, and nonlinear optical properties, Mol. Phys., 113 (2015) 3296–3302. https://doi.org/10.1080/00268976.2015.1018356

[50] M. T. H. Tarafder, A. Kasbollah, K. A. Crouse, A. M. Ali, B. M. Yamin, H. K. Fun, Synthesis and characterization of Zn(II) and Cd(II) complexes of S-Benzyl-β-N-(2-Pyridyl) methylenedithiocarbazate (HNNS): Bioactivity of the HNNS Schiff base and its Zn(II), Cu(II) and Cd(II) complexes and the X-Ray structure of the $[Zn(NNS)_2]$ complex, Polyhedron, 20 (2001) 2363–2370. https://doi.org/10.1016/S0277-5387(01)00817-8

[51] A. J. Gorczko, J. A. Szymura, The Prediction of relative abundance of isotopic clusters in mass spectrometry of coordination and organometallic compounds, Comput. Chem., 23 (1999) 135–142. https://doi.org/10.1016/S0097-8485(98)00035-7

[52] T. Yamada, H. Takahashi, R. Hatano, A novel insecticide, acetamiprid, in nicotinoid insecticides and the nicotinic acetylcholine receptor; I. Yamamoto, J.E. Casida, Eds.; Springer Japan: Tokyo, pages 149–176, 1999. https://doi.org/10.1007/978-4-431-67933-2_7

[53] D. Belkhir-Talbi, M. Makhloufi-Chebli, S. Terrachet-Bouaziz, D. Hikem-Oukacha, N. Ghemmit, L. Ismaili, A. M. S. Silva, M. Hamdi, Synthesis, characterization, theoretical studies, ADMET and drug-likeness analysis: Electrochemical and biological activities of metal complexes of 3-(2-Hydroxybenzoyl)-2H-Chromen-2-One, J. Mol. Struct., 1179 (2019) 495–505. https://doi.org/10.1016/j.molstruc.2018.11.035

[54] O. Alaysuy, H. M. Abumelha, A. Alsoliemy, A. Alharbi, N. M. Alatawi, H. E. M. Osman, R. Zaky, N. M. El-Metwaly, Elucidating of new hydrazide-based complexes derived from Pd(II), Cu(II) and Cd(II) ions: Studies concerning spectral, DFT, Hirshfeld-Crystal, biological screening beside Swiss-ADME verification, J. Mol. Struct., 1259 (2022) 132748. https://doi.org/10.1016/j.molstruc.2022.132748

[55] Gaines, T. B. Acute toxicity of pesticides, Toxicol. Appl. Pharmacol., 14 (1969) 515–534. https://doi.org/ 10.1016/0041-008X(69)90013-1